

# A molecular switch in RCK2 triggers sodium-dependent activation of $K_{Na}1.1$ (KCNT1) potassium channels

Bethan A. Cole,<sup>1</sup> Antreas C. Kalli,<sup>2,3</sup> Nadia Pilati,<sup>4</sup> Stephen P. Muench,<sup>1,3</sup> and Jonathan D. Lippiat<sup>1,\*</sup>

<sup>1</sup>School of Biomedical Sciences, University of Leeds, Leeds, United Kingdom; <sup>2</sup>Leeds Institute of Cardiovascular and Metabolic Medicine, University of Leeds, Leeds, United Kingdom; <sup>3</sup>Astbury Centre for Structural and Molecular Biology, University of Leeds, Leeds, United Kingdom; and <sup>4</sup>Autifony Srl, Padova, Italy

**ABSTRACT** The  $Na^+$ -activated  $K^+$  channel  $K_{Na}1.1$ , encoded by the *KCNT1* gene, is an important regulator of neuronal excitability. How intracellular  $Na^+$  ions bind and increase channel activity is not well understood. Analysis of  $K_{Na}1.1$  channel structures indicate that there is a large twisting of the  $\beta N$ - $\alpha Q$  loop in the intracellular RCK2 domain between the inactive and  $Na^+$ -activated conformations, with a lysine (K885, human subunit numbering) close enough to potentially form a salt bridge with an aspartate (D839) in  $\beta L$  in the  $Na^+$ -activated state. Concurrently, an aspartate (D884) adjacent in the same loop adopts a position within a pocket formed by the  $\beta O$  strand. In carrying out mutagenesis and electrophysiology with human  $K_{Na}1.1$ , we found that alanine substitution of selected residues in these regions resulted in almost negligible currents in the presence of up to 40 mM intracellular  $Na^+$ . The exception was D884A, which resulted in constitutively active channels in both the presence and absence of intracellular  $Na^+$ . Further mutagenesis of this site revealed an amino acid size-dependent effect. Substitutions at this site by an amino acid smaller than aspartate (D884V) also yielded constitutively active  $K_{Na}1.1$ , and D884I had  $Na^+$  dependence similar to wild-type  $K_{Na}1.1$ , while increasing the side-chain size larger than aspartate (D884E or D884F) yielded channels that could not be activated by up to 40 mM intracellular  $Na^+$ . We conclude that  $Na^+$  binding results in a conformational change that accommodates D884 in the  $\beta O$  pocket, which triggers further conformational changes in the RCK domains and channel activation.

**SIGNIFICANCE** Sodium-activated potassium channels regulate neuronal excitability, and their dysfunction causes severe childhood disorders. Here, we identify a structural determinant in the intracellular domains that is responsible for triggering channel activation in response to sodium ion binding. An increase in the size of a particular amino acid renders the channel sodium insensitive, while a decrease in size enables the channel to activate in the absence of sodium. This enhances our understanding of how this subclass of potassium channels respond to changes in the intracellular ionic environment. Furthermore, this may also further our understanding of the basis of human neurological disorders and their treatment.

## INTRODUCTION

$Na^+$ -activated  $K^+$  ( $K_{Na}$ ) channels open in response to elevation in the cytoplasmic  $Na^+$  concentration, contributing to hyperpolarization of the membrane potential of neurons and other cell types.  $K_{Na}1.1$  and  $K_{Na}1.2$  (or SLACK and SLICK) are members of the large-conductance, regulator

of  $K^+$  conductance (RCK) domain-containing subfamily of  $K^+$  channels and are activated by intracellular  $Na^+$  (1). Intracellular  $Na^+$  is an essential determinant of wild-type (WT)  $K_{Na}1.1$  channel opening, and in normal physiology,  $K_{Na}1.1$  activity is coupled to persistent inward  $Na^+$  currents, for example, through re-opening voltage-gated  $Na^+$  channels or NALCN channels that increase local  $Na^+$  concentration above that of the bulk cytosol (2,3). Additionally, transient currents through AMPA receptors located in the vicinity of  $K_{Na}1.1$  have also been implicated as a  $Na^+$  source for the channel as part of a negative feedback loop (4). The importance of these channels is highlighted by the seizure disorders and intellectual disability caused by pathogenic

Submitted October 11, 2023, and accepted for publication April 8, 2024.

\*Correspondence: [j.d.lippiat@leeds.ac.uk](mailto:j.d.lippiat@leeds.ac.uk)

Bethan A. Cole's present address is Nuffield Department of Clinical Neurosciences, University of Oxford, Oxford, United Kingdom.

Editor: Brad Rothberg.

<https://doi.org/10.1016/j.bpj.2024.04.007>

© 2024 Biophysical Society.

This is an open access article under the CC BY license (<http://creativecommons.org/licenses/by/4.0/>).



variants in either of the  $K_{Na}$ -encoding genes, *KCNT1* or *KCNT2* (5–9). In most cases, pathogenic variants in either gene result in a missense mutation that leads to enhanced  $K_{Na}$  channel activity, but loss of function is also found with some *KCNT2* variants (10). Quinidine, bepridil, and clofilium were the first drugs to be identified as  $K_{Na}$  channel inhibitors, with bithionol, riluzone, loxapine, and niclosamide as activators (11–13). Each of these drugs is nonselective and unlikely to be of clinical use in  $K_{Na}$  disorders. In response to *KCNT1* gain-of-function disorders, several groups have identified novel  $K_{Na}$ 1.1 channel inhibitors (14–16). Our approach exploited  $K_{Na}$  channel structures and targeted the pore domain in virtual high-throughput screening (14), but it is conceivable that future structure-based screening could instead target the  $Na^+$ -activation mechanism, which could improve specificity. However, the structural basis of how  $Na^+$  ions interact with  $K_{Na}$  channels and how this results in channel activation remains unknown.

Previously, residues located in the rat  $K_{Na}$ 1.1 RCK2 domain were proposed to form a  $Na^+$ -binding site based upon a  $Na^+$  coordination motif, DXRXXH, that is found in  $Na^+$ -activated GIRK channels (17). Mutating D818 and, to a lesser degree, H823 diminished rat  $K_{Na}$ 1.1  $Na^+$  activation when the channels were expressed and recorded from patches excised from *Xenopus* oocytes. In general,  $Na^+$  sensitivity was shifted to higher concentrations for channels mutated at either site (17). In human  $K_{Na}$ 1.2, mutation of the equivalent aspartate residue, D757, to arginine abolished  $Na^+$  activation in whole *Xenopus* oocytes, with function rescued by application of the activator niflumic acid (18). The structures of the chicken  $K_{Na}$ 1.1 channel in the closed (zero  $Na^+$  conditions) and activated (high  $Na^+$  conditions) conformations have since been resolved by cryo-electron microscopy (cryo-EM) and single-particle averaging (19,20), in which the  $Na^+$ -binding fold proposed by Zhang and others (17) was not evident. The region containing the proposed DXRXXH coordination motif is conserved between chicken and rat  $K_{Na}$ 1.1 but remains as a static loop in both the active and inactive conformations, as will be described below. Since  $Na^+$  ions, owing to their size, are usually unresolved in structures generated by cryo-EM, it is not known where in the channel they bind and how this results in increased channel activity.

In studying the cryo-EM structures of the inactive and active chicken  $K_{Na}$ 1.1 channel subunits, we identified a conformational difference between the two that we hypothesized could underlie  $Na^+$ -dependent activation. Furthermore, it appeared to involve the aspartate residue identified by Zhang and others (17) in playing a conformation-stabilizing role. Using site-directed mutagenesis and electrophysiology, we identify additional residues in a nearby region that are critical for  $Na^+$ -dependent activation and propose that a twisting of a loop between  $\beta$ N and  $\alpha$ Q in RCK2 acts as a molecular switch that underlies  $K_{Na}$ 1.1 acti-

vation. While preparing this manuscript, complementary studies on  $K_{Na}$ 1.1  $Na^+$  binding and activation were published, involving molecular dynamics simulations and mutagenesis (21) or cryo-EM (22), together with functional characterization. In presenting and discussing our findings, we highlight where our interpretation is consistent or conflicts with the conclusions of either of these studies.

## MATERIALS AND METHODS

### Analysis of protein structures

Structures of chicken  $K_{Na}$ 1.1 in the  $Na^+$ -activated (PDB: 5U70) and  $Na^+$ -free (PDB: 5U76) states (20) were analyzed and figures prepared using UCSF Chimera (23). Amino acid substitutions were introduced in silico using the Rotamer function and assessed using the Find Clashes/Contacts function. Initially, the rotamer with the highest probability, with respect to the chi parameters generated from the integrated Dunbrack 2010 library, was selected. If intramodel atomic clashes were obtained, then the next two rotamers in the probability ranking were evaluated. Molecular surfaces were calculated using the MSMS tool within Chimera (24).

### Molecular biology and transfection

The full-length pcDNA6- $K_{Na}$ 1.1 mammalian expression plasmid that we described previously (14) was used in these studies. Mutations were designed and introduced by polymerase chain reaction using the New England Biolabs method and confirmed by sequencing (Genewiz, Takeley, UK). Due to the large size and high GC content of the insert, mutations were generated in a plasmid containing the SbfI/BsiWI restriction fragment and then subcloned into the corresponding sites in the pcDNA6- $K_{Na}$ 1.1 construct. Chinese hamster ovary (CHO) cells were cultured in Dulbecco's modified Eagle's medium (Gibco, Paisley, UK) supplemented with 10% (v/v) fetal bovine serum, 50 U/mL penicillin, and 0.05 mg/mL streptomycin and incubated at 37°C in 5%  $CO_2$ . Cells were cotransfected with WT or mutated pcDNA6- $K_{Na}$ 1.1 together with pEYFP-N1 plasmid using Mirus TransIT-X2 reagent (Genflow, Lichfield, UK). For electrophysiological experiments, cells were plated onto borosilicate glass cover slips and used 2–4 days later.

### Electrophysiology

All chemicals were obtained from Sigma-Aldrich (Gillingham, UK) unless stated otherwise. Micropipettes were pulled from thin-walled borosilicate glass (Harvard Apparatus, Kent, UK), polished, and gave resistances of 1.5–2.5 M $\Omega$  in the experimental solutions. The bath (extracellular) solution contained, in mM, 140 NaCl, 1 CaCl<sub>2</sub>, 5 KCl, 29 glucose, 10 HEPES, and 1 MgCl<sub>2</sub> (pH 7.4) with NaOH. The 40 mM  $Na^+$  pipette (intracellular) solution contained, in mM, 130 K-gluconate, 30 NaCl, 29 glucose, 5 EGTA, and 10 HEPES (pH 7.3) with KOH. To obtain pipette solutions containing  $Na^+$  at 10 and 0 mM (nominally  $Na^+$  free), the NaCl was replaced by equimolar amounts of choline chloride.  $K_{Na}$ 1.1 activators loxapine succinate and niclosamide were prepared as 10 mM stock solutions in DMSO. The final drug concentrations were obtained by diluting the stock solution in the bath solution on the day of the experiment.

Currents were recorded from EYFP-fluorescing cells at room temperature (20°C–22°C) in the whole-cell patch-clamp configuration using an EPC10 amplifier (HEKA Electronics, Lambrecht, Germany), with >70% series resistance compensation (where appropriate), 2.9 kHz low-pass filtering, and 10 kHz digitization. Following the establishment of the whole-cell configuration, cells were held at –80 mV, and 400 ms voltage pulses from –100 to +80 mV in 10 mV increments were applied. With experiments that examine the effect of pharmacological activation, the 10 mM

NaCl pipette solution was used, and the voltage protocol was applied both before and after bath perfusion of 30  $\mu$ M of either niclosamide or loxapine.

## Data analysis

Samples were not randomized, and the experiments were not blinded. Data are presented as mean  $\pm$  SEM from  $n$  number of cells. Statistical analysis was performed using SPSS (IBM Analytics, Portsmouth, UK), with the chosen tests indicated in the figure legends;  $p < 0.05$  was considered significant. Without a priori knowledge of effect sizes, power calculations were not conducted. Representative whole-cell current traces were plotted and residual capacitance spikes removed in OriginPro. Whole-cell current-voltage relationships were divided by whole-cell capacitance to give the current density (pA/pF). Reversal potentials were obtained by fitting the linear part of current-voltage relationships around the reversal potential using linear regression and determining the voltage at the zero-current level. Conductance values ( $G$ ) at each voltage ( $V_m$ ) were obtained by dividing current amplitudes ( $I$ ) by the driving force on  $K^+$  ions, calculated using the reversal potentials ( $V_{rev}$ ) obtained in individual recordings:  $G = I/(V_m - V_{rev})$ . The conductance values were plotted against  $V_m$  and fitted with a Boltzmann function,  $G = (G_{max} - G_{min})/(1 + e^{(V_m - V_{0.5})/k}) + G_{min}$ , which gave values for activation midpoint ( $V_{0.5}$ ),  $G_{max}$ ,  $G_{min}$ , and the Slope factor ( $k$ ). Data were normalized by dividing by  $G_{max}$  for each experiment. Reported  $V_{0.5}$  values were corrected for liquid junction potential error after the experiment. With  $k = RT/zF$ , the valence of the gating charge,  $z$ , was estimated.

## RESULTS

### Identification of a putative $Na^+$ -binding site in $K_{Na}1.1$ structural data

The aspartate residue found by Zhang and others (17) to be critical for  $Na^+$  activation in rat  $K_{Na}1.1$ , D818, is equivalent to D812 in chicken and D839 in human  $K_{Na}1.1$ . To assist comparisons between studies of  $K_{Na}1.1$  clones from different species, the positions of the amino acids detailed in this study in human, rat, and chicken are provided in Table S1. We hereon refer only to the amino acid numbering in human  $K_{Na}1.1$ . The proposed  $Na^+$ -coordinating motif, based on that in GIRK channels, is conserved between species and forms the loop between  $\beta$ L and  $\alpha$ O in the  $K_{Na}1.1$  RCK2 domain. Firstly, the  $Na^+$ -binding fold proposed by the molecular modeling and simulations of RCK2 of the rat  $K_{Na}1.1$  (17) subunit was not observed in the cryo-EM structures of either the active (PDB: 5U70; Fig. 1 A) or inactive (PDB: 5U76) chicken  $K_{Na}1.1$  channels. Secondly, there was no discernible difference between the two structures in the positioning of the side chain of this aspartate or any of the neighboring residues previously proposed to contribute to  $Na^+$  binding (D839 in Fig. 1 B). Notably, in the structure of the  $Na^+$ -activated state, a lysine residue in the loop between  $\beta$ N- $\alpha$ Q (K885 in Fig. 1 B) falls within 3.4 Å of the aspartate, sufficiently close to form a salt bridge. In the apo state, this loop is not fully resolved, indicating disorder, but comparison with the structure of the activated state suggests that upon activation by sodium, there is a rotation of this loop around the axis of the backbone by approximately 180°. This was observed by Zhang and others (22) to be the

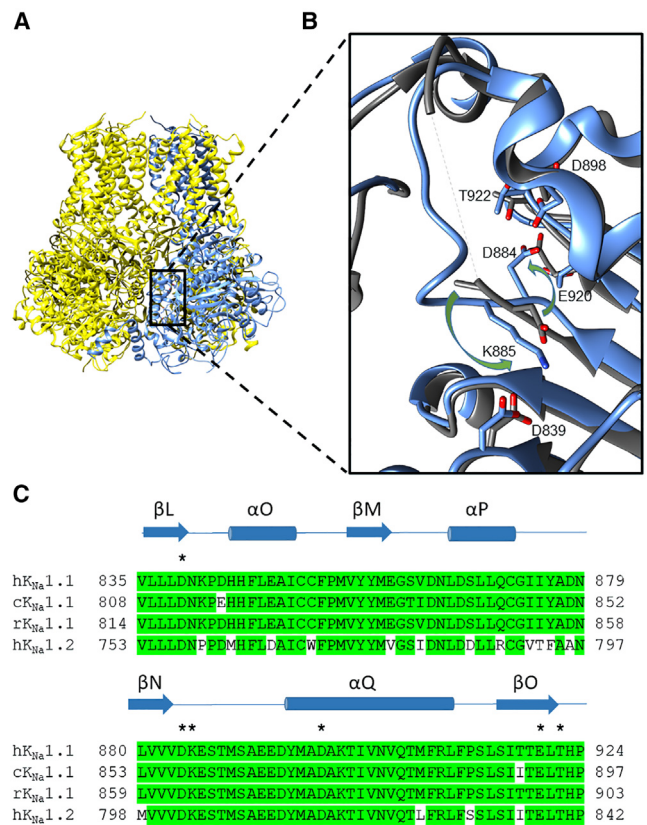


**FIGURE 1** Structural analysis of the  $Na^+$ -binding site proposed by Zhang and others (17) in chicken  $K_{Na}1.1$  channel protein resolved using cryo-EM. (A) Structure of chicken  $K_{Na}1.1$  in the active conformation (PDB: 5U70) with one subunit in the tetramer colored blue. Each subunit comprises six transmembrane helices (*top part of structure*) and a re-entrant P-loop between S5 and S6 that forms the  $K^+$ -selective filter. The large intracellular domains contain a pair of RCK domains, RCK1 and RCK2 (*bottom part of structure*). The domain of interest in RCK2 is enclosed by the black box. (B) Enlarged representation of the domain of interest with the active (*blue*) and inactive (PDB: 5U76; *dark gray*) conformations overlaid. The aspartate identified by Zhang and others (17) is D839 (all human  $K_{Na}1.1$  numbering). The twisting of the loop between  $\beta$ N- $\alpha$ Q in RCK2, indicated by the green arrows, positions a lysine (K885) close enough to form a salt bridge with the purported  $Na^+$ -binding aspartate (D839) in the  $Na^+$ -activated state. Concurrently, an aspartate (D884) in the same loop adopts a position proximal to the  $\beta$ O strand and is flanked by E920 and T922. The complete  $\beta$ N- $\alpha$ Q loop is not resolved in the inactive state (*dashed line*), indicating disorder. (C) Sequence alignment of the domain of interest between  $K_{Na}1.1$  from human (h), chicken (c), and rat (r), plus the closely related human  $K_{Na}1.2$ . Conserved residues (with respect to h $K_{Na}1.1$ ) are shaded green. The domain structure (22) is shown by the blue shapes, and the amino acids labeled in (B) are indicated by asterisks.

case in the structures of human  $K_{Na}1.1$ . Consequentially, the adjacent aspartate in the same  $\beta$ N- $\alpha$ Q loop (D884 in Fig. 1 B) adopts a position within a pocket formed by the  $\beta$ O  $\beta$ -strand in RCK2 (Fig. 1 B). Specifically, the aspartate side chain occupies a crevice between the  $\beta$ -carbons of E920 and T922 side chains and the L921 backbone. The differences between the cryo-EM structures of chicken  $K_{Na}1.1$  in the inactive and  $Na^+$ -activated states therefore indicate that the rotation and stabilization of the  $\beta$ N- $\alpha$ Q loop is a conformational change in RCK2 upon  $Na^+$  binding.

## Activation of WT $K_{Na}1.1$ by intracellular $Na^+$ and pharmacological activators

Guided by  $K_{Na}1.1$  channel structural data, a combination of mutagenesis and whole-cell electrophysiology was used to investigate the involvement of residues in  $Na^+$ -dependent activation of the human  $K_{Na}1.1$  channel. In our hands, human  $K_{Na}1.1$  runs down within seconds in excised inside-out patches, leaving unitary or no currents. Therefore, to efficiently explore the effects on macroscopic  $K_{Na}1.1$  currents, we conducted whole-cell patch-clamp recordings from CHO cells expressing WT or mutant  $K_{Na}1.1$  using pipette solutions with different concentrations of  $Na^+$  and pharmacological activation to bypass  $Na^+$  activation and confirm the presence of relatively  $Na^+$ -insensitive channels. The antipsychotic drug loxapine and the antihelminthic drug niclosamide are potent activators of WT  $K_{Na}1.1$  with half-maximal activation concentration ( $EC_{50}$ ) of 4.4 and 2.9  $\mu M$ , respectively (13). Both drugs also reduce the voltage dependence of  $K_{Na}1.1$  activation, resulting in near-linear current-voltage relationships and increased inward current at voltages negative to the reversal potential (Fig. S1). Initially, niclosamide was selected to confirm function expression of “inactive” mutant channels. CHO cells are believed to have little or no endogenous ion conductance (25). However, when 30  $\mu M$  niclosamide was perfused into the bath, a current with density  $58.96 \pm 9.60$  pA/pF at +10 mV was recorded from nontransfected CHO cells, compared to  $1.49 \pm 0.67$  pA/pF at +10 mV prior to its application ( $n = 4$  and 5 cells, respectively). Though this current is relatively small in comparison to the exogenous  $K_{Na}1.1$  current (Fig. S1, A and B), this could confound the functional rescue of seemingly inactive  $K_{Na}1.1$  channels. The identity of the conductance and charge carrier evoked by niclosamide is unknown, but experiments ruled out  $K_{Na}1.1$ , since the current was not inhibited by 10  $\mu M$  bepridil (Fig. S1 C). The reversal potential ( $-73.30 \pm 0.85$  mV,  $n = 4$ ) would be consistent with a  $K^+$ -selective conductance, but no further experiments were conducted to characterize the current and its ion selectivity. Loxapine had no effect on the membrane conductance of nontransfected CHO cells (Fig. S1, A and B) and was therefore more suitable for these experiments.

Firstly, to replicate the importance of the previously proposed  $Na^+$  sensor, D839 was mutated to both glutamate and alanine. The D839E mutation, which lengthened the side chain without affecting the negative charge, gave currents that were qualitatively no different from WT  $K_{Na}1.1$ . The current-voltage relationships closely resembled the WT  $K_{Na}1.1$  channel with 10 and 40 mM intracellular  $Na^+$ , and no currents were recorded in 0 mM intracellular  $Na^+$  (Fig. 2 B). Consistent with Zhang and others (17), no currents were recorded in the presence of 0, 10, or 40 mM intracellular  $Na^+$  from D839A channels. Large, relatively voltage-independent currents were yielded upon perfusion of 30  $\mu M$  loxapine into the bath solution, confirming the presence of this  $Na^+$ -insensitive mutant  $K_{Na}1.1$  channel at the cell membrane (Fig. 2).

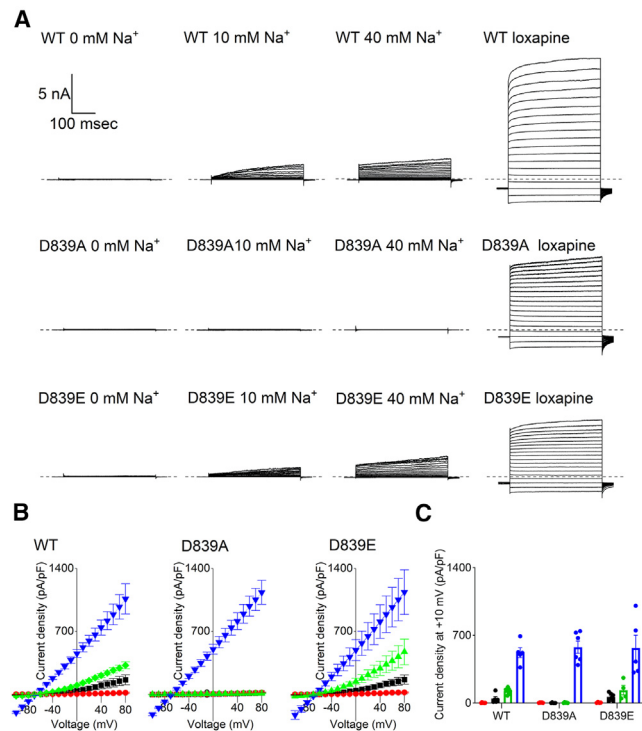


**FIGURE 2** Mutational analysis of the previously proposed  $Na^+$  sensor. (A) Representative whole-cell currents from CHO cells transfected with WT or mutant human  $K_{Na}1.1$ , with intracellular  $Na^+$  and drug exposure as indicated, in response to 400 ms steps from  $-100$  to  $+80$  mV in 10 mV increments from a holding potential of  $-80$  mV. The dashed lines indicate the zero-current level. (B) Mean ( $\pm$  SEM,  $n = 5$ –8 cells) current-voltage relationships for WT and mutant  $K_{Na}1.1$  channels in the presence of 0 (red circle), 10 (black square), and 40 (green diamond or green triangle) mM intracellular  $Na^+$  or 10 mM  $Na^+$  and 30  $\mu M$  loxapine (dark blue inverted triangle). (C) Mean bar with SEM and individual data points for current density at +10 mV from the data presented in (B), with the same color representation.

## The conformational change in the $\beta N$ - $\alpha Q$ loop and D884 controls the activation state of $K_{Na}1.1$ channels

The analysis of protein structures suggested that the movement of the D884 through the rotation of the  $\beta N$ - $\alpha Q$  loop could be a key step in the process of  $K_{Na}1.1$  activation by  $Na^+$ . Alternatively, through its negative charge, it could be a candidate for  $Na^+$  binding, so we mutated D884 to alanine. Unexpectedly, this resulted in a large increase in channel activity and apparent loss of  $Na^+$  dependence. The voltage-dependent currents recorded from CHO cells expressing D884A  $K_{Na}1.1$  with 0, 10, or 40 mM intracellular  $Na^+$  were all similar (Figs. 3 A and S2 A). Perfusion of 30  $\mu M$  loxapine to cells had little effect on the current amplitude apart from an apparent loss of voltage dependence, as indicated by a straightening of the current-voltage relationship (Fig. 3 B). Mutation of the same residue to valine, which has a longer side chain by just one carbon, had similar effects (Fig. 3). Activation midpoints derived from conductance-voltage relationships fitted with a Boltzmann

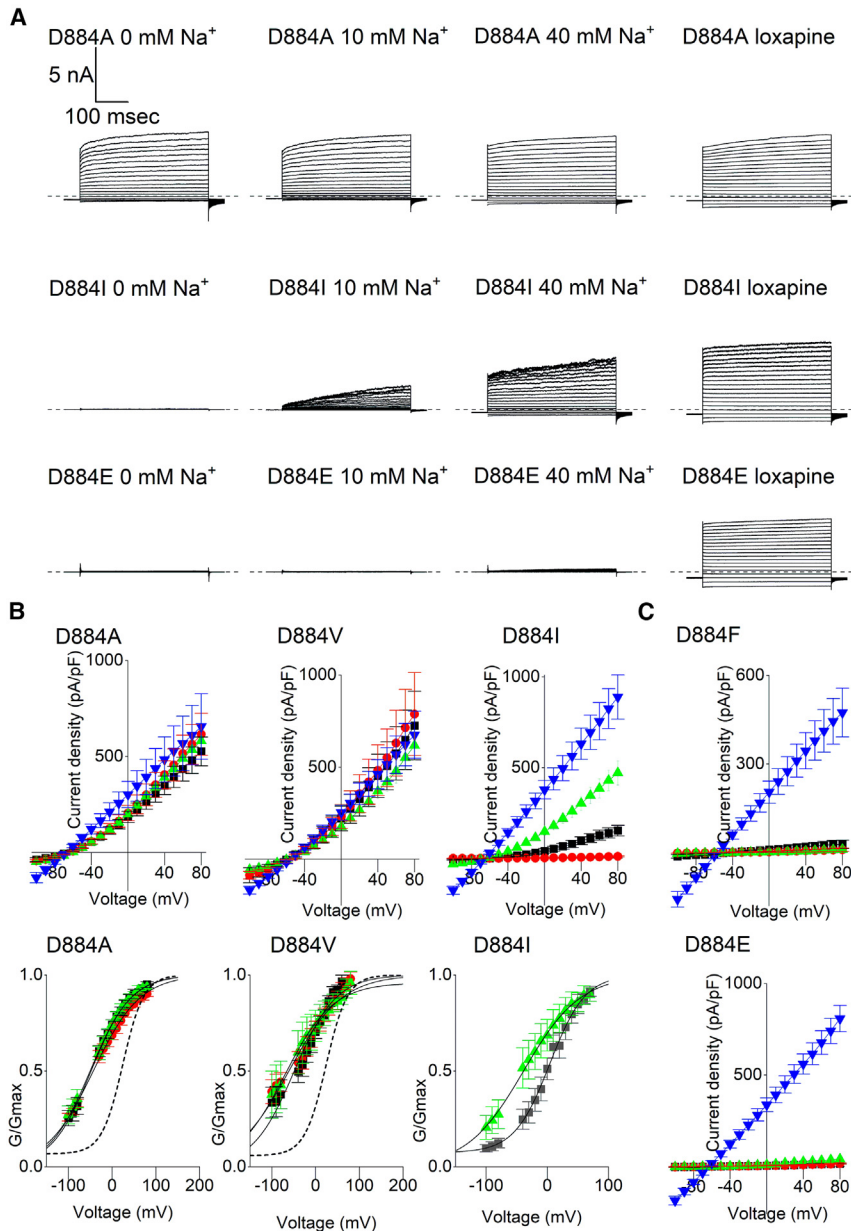


**FIGURE 3** Role of D884 in controlling  $K_{Na}1.1$  channel activation. (A) Representative D884A, D884I, and D884E  $K_{Na}1.1$  whole-cell currents in response to 400 ms steps from  $-100$  to  $+80$  mV in 10 mV increments from a holding potential of  $-80$  mV. The dashed lines indicate the zero-current level. (B) Mean  $\pm$  SEM ( $n = 5-8$  cells) current-voltage and conductance-voltage relationships for D884A, D884V, and D884I  $K_{Na}1.1$  with 0 (red circle), 10 (black square), and 40 (green diamond) mM intracellular  $Na^+$  or 10 mM  $Na^+$  and 30  $\mu$ M loxapine (dark blue inverted triangle). The mean conductance-voltage relationship for WT  $K_{Na}1.1$  recorded with 10 mM intracellular  $Na^+$  is indicated by a dotted line for comparison. (C) Mean  $\pm$  SEM current-voltage relationships for D884F and D884E  $K_{Na}1.1$  with 0 (red circle), 10 (black square), and 40 (green triangle) mM intracellular  $Na^+$  or 10 mM  $Na^+$  and 30  $\mu$ M loxapine (dark blue inverted triangle).

equation for D884A and D884V in 10 mM  $Na^+$  were significantly hyperpolarized compared to WT  $K_{Na}1.1$  (Table 1). With 40 mM intracellular  $Na^+$ , the activation midpoints for D884A and D884V  $K_{Na}1.1$  were not significantly different from WT  $K_{Na}1.1$  under the same conditions. While WT  $K_{Na}1.1$  currents were negligible with 0 mM intracellular  $Na^+$ , the activation midpoints for D884A and D884V with 0 mM  $Na^+$  were not significantly different from those obtained with 10 and 40 mM  $Na^+$  (Table 1).

Upon increasing the size of the hydrophobic sidechain further by mutating D884 to isoleucine and phenylalanine, different effects were observed. D884I  $K_{Na}1.1$  currents were similar to those obtained from WT  $K_{Na}1.1$  with each intracellular  $Na^+$  concentration tested (Figs. 3 B and S2 A;

Table 1). In contrast, no discernible current could be recorded from D884F  $K_{Na}1.1$  with any of the  $Na^+$  concentrations tested up to 40 mM, though function was rescued by loxapine application (Fig. 3 C). Finally, we mutated D884 to glutamate, which retained the negative charge but increased the side chain by one carbon. The D884E mutation in  $K_{Na}1.1$  had an effect similar to D884F, with negligible currents with 0, 10, and 40 mM intracellular  $Na^+$  each, but large whole-cell currents were recorded following the application of loxapine (Figs. 3, A–C, and S2 A).

These results suggested that it could be the size and not the charge of the side chain at amino acid position 884 that determined whether the  $K_{Na}1.1$  channel remained  $Na^+$  dependent or became locked in either the inactive or

**TABLE 1** Parameters derived from Boltzmann fit of WT and D884 mutant  $K_{Na1.1}$  channel conductance with 0, 10, and 40 mM intracellular  $Na^+$ 

$K_{Na1.1}$ variant	$[Na^+]_i$ (mM)	$V_{0.5}$ (mV)	$z$
WT	10	$2.15 \pm 3.69$	$0.81 \pm 0.09$
WT	40	$-46.63 \pm 8.06$	$0.75 \pm 0.14$
D884A	0	$-60.28 \pm 9.60$	$0.47 \pm 0.03$
D884A	10	$-61.92 \pm 6.77^a$	$0.60 \pm 0.07$
D884A	40	$-60.33 \pm 8.36$	$0.59 \pm 0.09$
D884V	0	$-46.99 \pm 11.08$	$0.61 \pm 0.07$
D884V	10	$-61.08 \pm 3.23^b$	$0.57 \pm 0.04$
D884V	40	$-60.86 \pm 4.89$	$0.57 \pm 0.08$
D884I	10	$0.23 \pm 6.78$	$0.92 \pm 0.02$
D884I	40	$-39.17 \pm 14.32$	$0.66 \pm 0.09$

Data are presented as mean  $\pm$  SEM ( $n = 5$ – $9$  cells).  $V_{0.5}$ , half-maximal activation voltage.

<sup>a</sup> $p < 0.0005$  compared to WT  $V_{0.5}$  with 10 mM intracellular  $Na^+$  (independent one-way ANOVA with Tukey's post hoc test).  $z$  was derived from the slope of the Boltzmann curve,  $RT/zF$ . No significant differences in  $z$  were found with mutant  $K_{Na1.1}$  compared to WT with either 10 or 40 mM intracellular  $Na^+$  (ANOVA).

<sup>b</sup> $p < 0.005$ .

$Na^+$ -activated state under these conditions. We returned to the structure of the  $Na^+$ -activated  $K_{Na1.1}$  channel and modeled the D884 mutations in silico. While aspartate and isoleucine at position 884 could be closely accommodated in the surrounding  $\beta O$  pocket, together with the smaller alanine and valine side chains with some leeway, substituting the larger glutamate and phenylalanine side chains resulted in steric clashes with T922 (Fig. 4). Additional energy minimization steps with the D884I model did not result in any discernable changes in orientation involving these side chains (Fig. S3 A). D884 was mutated to asparagine in rat  $K_{Na1.1}$  by Xu and others (21), resulting in  $Na^+$  insensitivity, and we found that this mutation could also result in a steric clash in silico (Fig. S3 B).

### The role of K885 and residues in or near the $\beta O$ strand in $Na^+$ activation

The structural analysis conducted above suggested that  $Na^+$  activation causes the  $\beta N$ - $\alpha Q$  loop to transition from a disordered state to a conformation that could potentially be stabilized by a salt bridge between D839 (studied above) and K885. To test this idea, K885 was neutralized to alanine. Like with D839A  $K_{Na1.1}$ , negligible currents were recorded from cells expressing K885A  $K_{Na1.1}$  with 0 and 10 mM intracellular  $Na^+$  (Figs. 5 and S2 B). A small current was recorded from K885A  $K_{Na1.1}$  when intracellular  $Na^+$  was elevated to 40 mM, suggesting a substantial decrease in  $Na^+$  sensitivity of the channel. Functional expression of K885A  $K_{Na1.1}$  channels was again confirmed by the addition of 30  $\mu M$  loxapine, which evoked large whole-cell currents comparable with those we observed earlier in the study.

We then questioned if the negatively charged (D898 and E920) or polar (T922) side chains in the vicinity of the

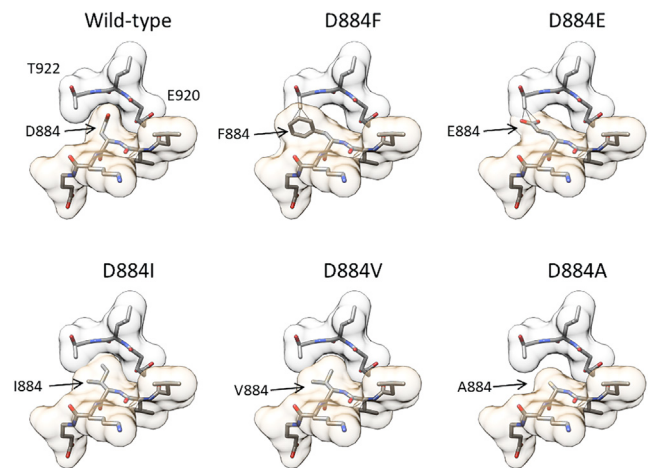


**FIGURE 4** Molecular modeling of D884 mutations. Models were generated from the structure of chicken  $K_{Na1.1}$  in the  $Na^+$ -activated state (PDB: 5U70), here with the numbering of conserved residues in human  $K_{Na1.1}$ . In each model, the pocket formed by  $^{920}ELT^{922}$  in the  $\beta O$  strand is shown with pale gray space fill, with  $^{882}VVDKE^{886}$  in the  $\beta N$ - $\alpha Q$  loop with pale gold space fill below. With the D884F and D884E substitutions, predicted atomic clashes between the substituted side chains and T922 are indicated by solid black lines. No clashes were predicted in the other models.

pocket accommodating D884 in the activated state played a role in activation by  $Na^+$ . Mutation of each of these to alanine similarly disrupted  $Na^+$  activation, with no significant currents recorded with 0, 10, or 40 mM intracellular  $Na^+$  (Figs. 5 and S2 B). Functional rescue was achieved with each of these mutant  $K_{Na1.1}$  channels following the application of 30  $\mu M$  loxapine. We initially considered whether these residues might contribute to a site for  $Na^+$  to occupy and activate the channel. To see if we could rescue one of these mutations, E920A, or attract D884 into this site and increase activity, D898 and T922 were mutated to the positively charged lysine. However, with each of the D898K, E920A/D898K, and T922K  $K_{Na1.1}$  channels, the effect was same as the alanine substitutions in this pocket (Figs. 5 and S2 B). Again, no currents were recorded with 0, 10, or 40 mM intracellular  $Na^+$ , and functional rescue was achieved with 30  $\mu M$  loxapine application. We found that mutation of D898 to either alanine or lysine appeared to result in a weak inward rectification in loxapine-evoked current-voltage relationships (Fig. 5 B).

### DISCUSSION

Our data suggest that the  $\beta N$ - $\alpha Q$  loop in RCK2 of  $K_{Na1.1}$  acts as a molecular switch controlling transitions between the  $Na^+$ -activated and  $Na^+$ -free inactive states. In the activated state, this loop may be stabilized by a salt bridge between K885 and D839. This explains why previous mutations of this aspartate, D812 in rat  $K_{Na1.1}$ , by Zhang and others (17) resulted in a loss of  $Na^+$  sensitivity, leading to their proposal that this formed a  $Na^+$ -binding site. Concurrently, the ability of D884 to occupy a pocket formed by the

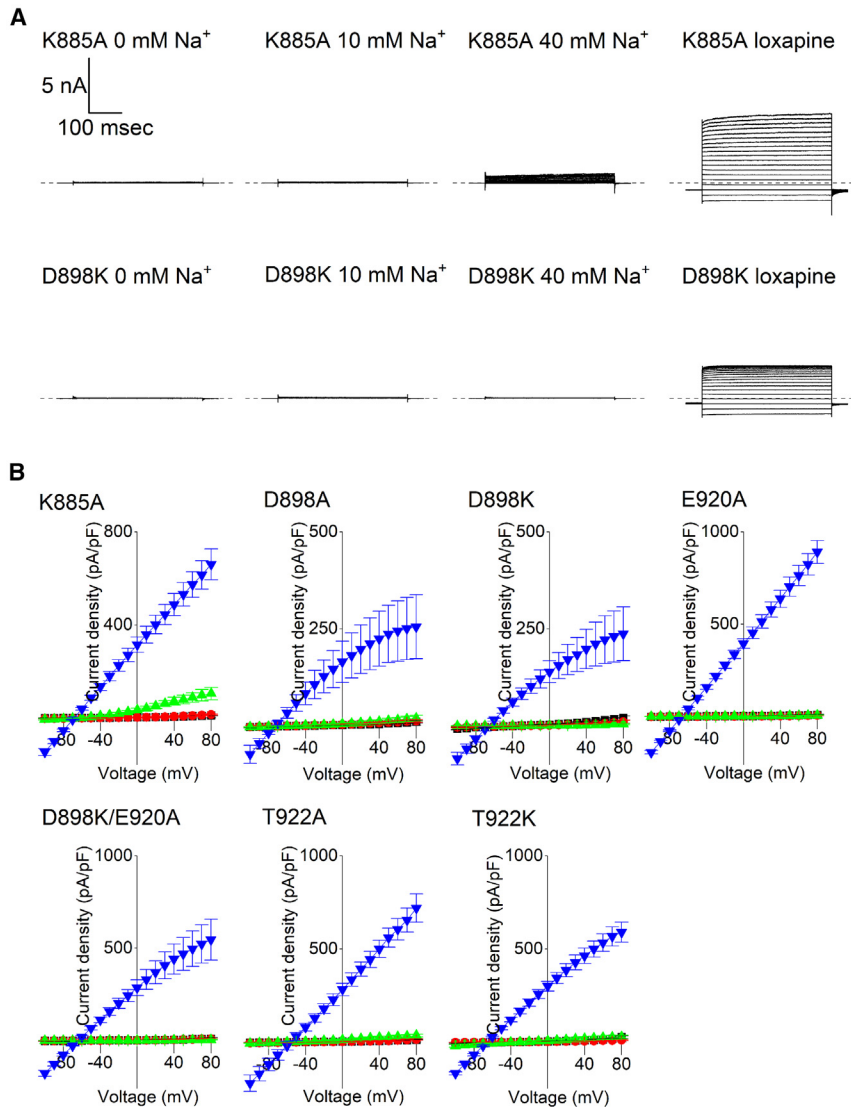


**FIGURE 5** Disruption of Na<sup>+</sup> activation through loss of a potential D839/K885 salt bridge and residues in or near  $\beta O$ . (A) Representative whole-cell K885A and D898K  $K_{Na}1.1$  currents in each condition, as indicated, in response to 400 ms steps from  $-100$  to  $+80$  mV in 10 mV increments from a holding potential of  $-80$  mV. The dashed lines indicate the zero-current level. (B) Mean ( $\pm$  SEM,  $n = 5-8$  cells) current-voltage relationships for mutated  $K_{Na}1.1$  channels in the presence of 0 (red circle), 10 (black square), and 40 (green triangle) mM intracellular Na<sup>+</sup> or 10 mM Na<sup>+</sup> and 30  $\mu$ M loxapine (dark blue inverted triangle).

$\beta O$  strand in the activated state appears to be important for activation. Mutating this side chain to either phenylalanine or glutamate prevented  $K_{Na}1.1$  channel activation by 40 mM intracellular Na<sup>+</sup>, but mutation to either alanine or valine caused the channel to adopt a constitutively activated, but voltage-gated, Na<sup>+</sup>-independent state. This could imply that the conformation adopted by this pocket in the absence of Na<sup>+</sup> prevents D884 and the  $\beta N$ - $\alpha Q$  loop from adopting the stabilized state but can accommodate alanine and valine side chains in place of D884. This domain is highly conserved between  $K_{Na}1.1$  and  $K_{Na}1.2$ , including each of the residues described here (Fig. 1 A), indicating a common mechanism.

One possible explanation for the different effects of the mutations relates solely to the size of the side chain at position D884, as considered in the *in silico* mutagenesis (Fig. 4). However, the amino acid substitutions may have wider-reaching effects on the protein structure through changes to the

electrostatics in the locality of this region. Rather than promoting (D884A, D884V) or preventing (D884F, D884E) the adoption of the Na<sup>+</sup>-activated conformation, converse effects of these mutations on the apo state might underlie these effects. Furthermore, given the near 180° rotation of the  $\beta N$ - $\alpha Q$  loop between these two states, the mutations may affect the intervening conformational dynamics.

D884 was recently proposed by both Xu and others (21) and Zhang and others (22) to contribute to a potential cation binding site. Mutating the equivalent of D884 in rat  $K_{Na}1.1$  to asparagine rendered the channel nonfunctional at intracellular Na<sup>+</sup> concentrations to up to 2 M (21). Consequently, and supported by molecular dynamics simulations, this aspartate was proposed as one of two Na<sup>+</sup>-binding sites in each subunit. In contrast, we found that the charge of this residue is not critical to  $K_{Na}1.1$  channel function, since D884I  $K_{Na}1.1$  channels behaved similarly to WT  $K_{Na}1.1$ . *In silico* mutagenesis of this aspartate in the chicken  $K_{Na}1.1$  structure to asparagine

caused a steric clash with acidic pocket residues, similar to D884E and D884F, substitutions of which prevented  $\text{Na}^+$  activation in our experiments. This explains the lack of activity with the asparagine mutation observed by Xu and others (21). D884 is part of cation-binding “site 2” identified by Zhang and others (22), who also studied the D884A  $\text{K}_{\text{Na}}1.1$  mutation. Using intracellular  $\text{Na}^+$  concentrations upwards from 100 mM, they found a fourfold decrease in the  $\text{Na}^+$   $\text{EC}_{50}$ . Since we recorded activated  $\text{K}_{\text{Na}}1.1$  channel currents in the absence of  $\text{Na}^+$ , the residual  $\text{Na}^+$  dependence may arise from an alternative  $\text{Na}^+$ -binding site with these higher concentrations. The anomalous density in cation site 2 of human  $\text{K}_{\text{Na}}1.1$  described by Zhang and others (22) was attributed to a  $\text{K}^+$  ion coordinated simultaneously by D839 and D884. This protein structure was obtained in  $\text{Na}^+$ -free and KCl-rich conditions and attributed to the closed or inactive conformation. The structure of this region in the activated or open human  $\text{K}_{\text{Na}}1.1$  described in the same study is similar to that obtained with the chicken homolog (Fig. 1), where D884 is effectively replaced by K885 upon the conformational change in the  $\beta\text{N}$ - $\alpha\text{Q}$  loop, together with a loss of anomalous density in site 2. The significance of  $\text{K}^+$  binding to this site in the inactive conformation is not known, but it is important to note that it is vacated by D884 upon  $\text{Na}^+$  activation.

We are unable to propose a specific  $\text{Na}^+$ -binding site from our investigation, but mutagenesis of residues D898, E920, and T922 that also disrupted  $\text{Na}^+$  activation would support the idea that  $\text{Na}^+$  binds in this region. These residues may have a role in coordinating  $\text{Na}^+$  ions, consistent with E920 having been identified by Xu and others (21) as a  $\text{Na}^+$ -coordinating side chain, and may underlie the structural change required to accommodate D884 by the  $\beta\text{O}$  strand. Mutation of one of these residues, D898, to either lysine or alanine resulted in inward rectification of the  $\text{K}_{\text{Na}}1.1$  current-voltage relationship when activated by loxapine. It was noted in the structure of the chicken  $\text{K}_{\text{Na}}1.1$  channel that the ring of RCK domains forms a “funnel” that narrows as it approaches the pore-forming region and has a largely electronegative surface (19). D898 contributes to this highly negatively charged surface, which may contribute to ion conduction. The negatively charged residues are thought to attract  $\text{K}^+$  ions and contribute to the relatively high  $\text{K}^+$  conductance of this and other members of the channel subfamily, and mutation of D898 may have an effect of outward  $\text{K}^+$  currents, leading to the slight inward rectification observed.

Consistent with the model presented here, the rotation and adoption of a stable  $\alpha$ -helix by the  $\beta\text{N}$ - $\alpha\text{Q}$  loop in RCK2 in the activated, but disordered in the  $\text{Na}^+$ -free,  $\text{K}_{\text{Na}}1.1$  conformation were highlighted in the recently published structure of human  $\text{K}_{\text{Na}}1.1$  (17). The authors argue that this conformational change influences interactions between RCK2 and RCK1 domains, resulting in the overall expansion that opens the channel gate. In conclusion, this structural and our functional data point to this loop as the key regulator of  $\text{K}_{\text{Na}}$  channel activation by  $\text{Na}^+$ . The constitutive activity with the

D884A and D884V mutant  $\text{K}_{\text{Na}}1.1$  in the absence of  $\text{Na}^+$  provide further clues as to how this channel is regulated. Given that these mutant channels, with the smaller side chain, are able to activate without  $\text{Na}^+$ , this indicates that the WT channel is primed for activation but requires a small structural change caused by  $\text{Na}^+$  binding to enable the  $\beta\text{N}$ - $\alpha\text{Q}$  loop to adopt the activated state. It is this inactive but primed state that may be disrupted by inherited mutations that result in  $\text{K}_{\text{Na}}1.1$  gain of function.

## DATA AND CODE AVAILABILITY

The unique reagents generated during this study are available upon reasonable request to the corresponding author. No additional data are associated with this article.

## SUPPORTING MATERIAL

Supporting material can be found online at <https://doi.org/10.1016/j.bpj.2024.04.007>.

## AUTHOR CONTRIBUTIONS

B.A.C., J.D.L., A.C.K., and S.P.M. designed the study. B.A.C. and J.D.L. performed research. B.A.C., J.D.L., A.C.K., S.P.M., and N.P. analyzed and interpreted data. B.A.C. and J.D.L. drafted the manuscript. B.A.C., J.D.L., A.C.K., S.P.M., and N.P. edited and approved the manuscript.

## ACKNOWLEDGMENTS

This work was supported by a BBSRC-CASE PhD studentship awarded to B.A.C. (BB/M011151/1) and Autifony Therapeutics Ltd.. For the purpose of open access, the authors have applied a creative commons attribution (CC BY) license to any author-accepted manuscript version arising from this submission.

## DECLARATION OF INTERESTS

The authors declare no competing interests.

## REFERENCES

1. Yuan, A., C. M. Santi, ..., L. Salkoff. 2003. The sodium-activated potassium channel is encoded by a member of the Slo gene family. *Neuron*. 37:765–773.
2. Hage, T. A., and L. Salkoff. 2012. Sodium-activated potassium channels are functionally coupled to persistent sodium currents. *J. Neurosci*. 32:2714–2721.
3. Li, P., C. M. Halabi, ..., L. Salkoff. 2019. Sodium-activated potassium channels moderate excitability in vascular smooth muscle. *J. Physiol*. 597:5093–5108.
4. Nanou, E., A. Kyriakatos, ..., A. El Manira. 2008.  $\text{Na}^+$ -mediated coupling between AMPA receptors and  $\text{K}_{\text{Na}}$  channels shapes synaptic transmission. *Proc. Natl. Acad. Sci. USA*. 105:20941–20946.
5. Kessi, M., B. Chen, ..., F. Yin. 2020. Intellectual Disability and Potassium Channelopathies: A Systematic Review. *Front. Genet*. 11:614.



6. Bonardi, C. M., H. O. Heyne, ..., G. Rubboli. 2021. KCNT1-related epilepsies and epileptic encephalopathies: phenotypic and mutational spectrum. *Brain*. 144:3635–3650.
7. Barcia, G., M. R. Fleming, ..., R. Nabbout. 2012. De novo gain-of-function KCNT1 channel mutations cause malignant migrating partial seizures of infancy. *Nat. Genet.* 44:1255–1259.
8. Heron, S. E., K. R. Smith, ..., L. M. Dibbens. 2012. Missense mutations in the sodium-gated potassium channel gene KCNT1 cause severe autosomal dominant nocturnal frontal lobe epilepsy. *Nat. Genet.* 44:1188–1190.
9. Mao, X., N. Bruneau, ..., L. Aniksztejn. 2020. The Epilepsy of Infancy With Migrating Focal Seizures: Identification of de novo Mutations of the KCNT2 Gene That Exert Inhibitory Effects on the Corresponding Heteromeric K(Na)<sub>1.1</sub>/K(Na)<sub>1.2</sub> Potassium Channel. *Front. Cell. Neurosci.* 14:1.
10. Cioclu, M. C., I. Mosca, ..., M. Tagliatela. 2023. KCNT2-Related Disorders: Phenotypes, Functional, and Pharmacological Properties. *Ann. Neurol.* 94:332–349.
11. Yang, B., V. K. Gribkoff, ..., L. K. Kaczmarek. 2006. Pharmacological activation and inhibition of Slack (Slo2.2) channels. *Neuropharmacology*. 51:896–906.
12. de Los Angeles Tejada, M., K. Stolpe, ..., D. A. Klaerke. 2012. Clofilium inhibits Slick and Slack potassium channels. *Biologics*. 6:465–470.
13. Biton, B., S. Sethuramanujam, ..., P. Avenet. 2012. The antipsychotic drug loxapine is an opener of the sodium-activated potassium channel slack (Slo2.2). *J. Pharmacol. Exp. Therapeut.* 340:706–715.
14. Cole, B. A., R. M. Johnson, ..., J. D. Lippiat. 2020. Structure-Based Identification and Characterization of Inhibitors of the Epilepsy-Associated KNa1.1 (KCNT1) Potassium Channel. *iScience*. 23:101100.
15. Spitznagel, B. D., N. M. Mishra, ..., C. D. Weaver. 2020. VU0606170, a Selective Slack Channels Inhibitor, Decreases Calcium Oscillations in Cultured Cortical Neurons. *ACS Chem. Neurosci.* 11:3658–3671.
16. Griffin, A. M., K. M. Kahlig, ..., G. Martinez-Botella. 2021. Discovery of the First Orally Available, Selective KNa1.1 Inhibitor: In Vitro and In Vivo Activity of an Oxadiazole Series. *ACS Med. Chem. Lett.* 12:593–602.
17. Zhang, Z., A. Rosenhouse-Dantsker, ..., D. E. Logothetis. 2010. The RCK2 domain uses a coordination site present in Kir channels to confer sodium sensitivity to Slo2.2 channels. *J. Neurosci.* 30:7554–7562.
18. Thomson, S. J., A. Hansen, and M. C. Sanguinetti. 2015. Identification of the Intracellular Na<sup>+</sup> Sensor in Slo2.1 Potassium Channels. *J. Biol. Chem.* 290:14528–14535.
19. Hite, R. K., P. Yuan, ..., R. MacKinnon. 2015. Cryo-electron microscopy structure of the Slo2.2 Na(+)-activated K(+) channel. *Nature*. 527:198–203.
20. Hite, R. K., and R. MacKinnon. 2017. Structural Titration of Slo2.2, a Na<sup>+</sup>-Dependent K<sup>+</sup> Channel. *Cell*. 168:390–399.e11.
21. Xu, J., Y.-T. Lv, ..., Z. Zhang. 2023. Identification of Sodium- and Chloride-Sensitive Sites in the Slack Channel. *J. Neurosci.* 43:2665–2681.
22. Zhang, J., S. Liu, ..., D. Jiang. 2023. Structural basis of human Slo2.2 channel gating and modulation. *Cell Rep.* 42:112858.
23. Pettersen, E. F., T. D. Goddard, ..., T. E. Ferrin. 2004. UCSF Chimera—a visualization system for exploratory research and analysis. *J. Comput. Chem.* 25:1605–1612.
24. Sanner, M. F., A. J. Olson, and J. C. Spehner. 1996. Reduced surface: an efficient way to compute molecular surfaces. *Biopolymers*. 38:305–320.
25. Gamper, N., J. D. Stockand, and M. S. Shapiro. 2005. The use of Chinese hamster ovary (CHO) cells in the study of ion channels. *J. Pharmacol. Toxicol. Methods*. 51:177–185.